JOURNAL OF THEORETICAL AND APPLIED MECHANICS
57, 2, pp. 475-487, Warsaw 2019
DOI: 10.15632/jtam-pl/105467

STUDY OF THE ANTI-PLANE PROBLEM OF A DUGDALE-BARENBLATT CRACK IN A WELDED STRIP USING THE INTEGRAL EQUATION METHOD

Amine Brick Chaouche
Research Center in Industrial Technologies (CRTI), Algiers, Algeria
Department of Mechanics, Structures Laboratory, Saad Dahlab University, Blida, Algeria
e-mail: a.brick-chaouche@crti.dz

Hicheme Ferdjani
Department of Mechanics, Structures Laboratory, Saad Dahlab University, Blida, Algeria
e-mail: h_ferdjani@univ-blida.dz

Nacer Tala-Ighil
Research Center in Industrial Technologies (CRTI), Algiers, Algeria
e-mail: n.tala-ighil@crti.dz

The elasto-static anti-plane problem of a Dugdale-Barenblatt crack in a welded infinite strip is formulated in terms of a singular integral equation (SIE). The weld joint is modeled as a tri-material structure: the weld metal (WM), the base metal (BM) and the heat-affected zone (HAZ). The HAZ is modeled with an exponentially variable shear modulus. The SIE is solved using Tchebychev polynomials. The influence of the elastic mismatching (the ratio between the shear modulus of WM and BM) and width of the HAZ on the fracture load and on the crack propagation is investigated.

Keywords: crack, Dugdale-Barenblatt model, weld joint, singular integral equation, infinite strip

1. Introduction

Weld joints are considered as non-homogeneous structures in the fracture mechanics modeling. This non-homogeneity is due to variable elastic and mechanical properties across the joint. These structures are, in some cases, modeled as a bi-material structure taking into account the weld metal and the base metal only (Hao *et al.*, 1997; Zhang *et al.*, 1997a; Burstow *et al.*, 1997; Rakin *et al.*, 2008; Donato *et al.*, 2009). In other cases, they are modeled as a tri-material structure with, in addition, the heat affected zone (HAZ) (Zhang *et al.*, 1997b; Ranestad *et al.*, 1997; Hao *et al.*, 2000; Negre *et al.*, 2004). In some special cases, they are modeled as a four-material structure with, in addition, the fusion inter-diffusion zone (Li *et al.*, 2008).

Several papers treated the problem of a crack in a weld joint. Using the finite element method, Hao *et al.* (1997) studied the effect of strength mismatch on the limit load, and Donato *et al.* (2009) on the crack driving forces (J-integral and crack tip opening displacement CTOD). The effect of strength mismatch (the ratio between the strength of the HAZ and the weld metal WM) on the stress and strain fields near the crack tip was studied using both the slip-line field method and the finite element method in (Burstow *et al.*, 1997; Zhang *et al.*, 1997a; Hao *et al.*, 2000; Rakin *et al.*, 2008). Negre *et al.* (2004) carried out a finite element analysis to study the effect of strength mismatch on the applied load versus the crack driving force (in term of CTOD). Using an integral method, Li *et al.* (2008) investigated the effect of elastic mismatch on the computed stress intensity factor of a crack in the weldment.

This study is performed in the framework of the revisited Griffith theory (Francfort and Marigo, 1998) for brittle fracture. The Dugdale-Barenblatt model and the crack propagation criteria are established using an energy minimization principle with a surface energy density of Barenblatt type (Ferdjani and Marigo, 2015).

The propagation of a Dugdale-Barenblatt crack has been studied for different types of structures and loadings. For mode I case, Ferdjani *et al.* (2007) studied a crack in an infinite isotropic medium under uniform traction. For mode III case, Ferdjani (2008, 2013) and Ferdjani *et al.* (2009) considered a crack in a semi-infinite isotropic medium in an infinite isotropic strip, and at the interface of a strip and a half-plane constituted of different isotropic materials under uniform anti-plane shearing, respectively. For the mixed mode case, Ferdjani and Marigo (2015) studied a crack at the interface of a strip and a half-plane constituted of the same isotropic material under uniform traction. In the present paper, the anti-plane problem of a welded strip containing a Dugdale-Barenblatt crack parallel to its boundaries is studied.

The paper is organized as follows. The Dugdale-Barenblatt model is presented in Section 2. In Section 3, the studied structure is depicted and the crack propagation criteria presented. In Section 4, the singular integral equation is deduced and the resolution method exposed. Section 5 is devoted to a parametric study of the problem.

2. The Dugdale-Barenblatt model

In this model, the surface energy density Φ depends on the sliding displacement jump across the crack, unlike the Griffith model in which it is assumed to be constant (Fig. 1b). When assuming that the sliding of the crack is in mode III, the surface energy density is defined as

$$\phi([|w|]) = \begin{cases} \dfrac{1}{\delta_c} G_c [|w|] & \text{if} \quad [|w|] \leqslant \delta_c \\ G_c & \text{if} \quad [|w|] \geqslant \delta_c \end{cases} \tag{2.1}$$

where $[|w|]$ denotes the value of the sliding displacement jump in mode III, G_c is the critical energy release rate and δ_c is an internal length characteristic of the cohesive models. The ratio G_c/δ_c has the dimension of stress, and the critical stress of the material τ_c is given by

$$\tau_c = \frac{G_c}{\delta_c} \tag{2.2}$$

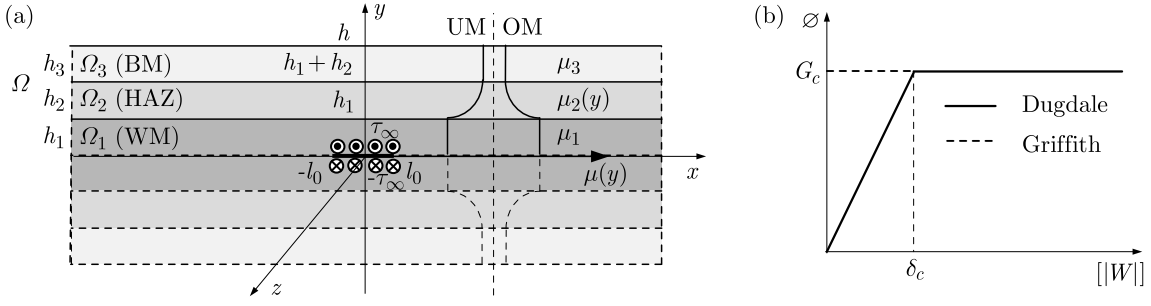

Fig. 1. (a) Studied structure (UM and OM refer to undermatching and overmatching cases respectively). (b) Surface energy density in the models of Dugdale-Barenblatt and Griffith

In terms of the cohesive forces, the tangential stress of interaction between the crack faces is equal to τ_c as long as the sliding $[|w|] < \delta_c$, and disappears as soon as $[|w|] > \delta_c$. Therefore, the crack faces are generally divided into two zones: the cohesive zone in which the cohesive forces are equal to τ_c and the non-cohesive zone in which there are no cohesive forces.

3. The studied structure

The studied structure is an infinite strip $\Omega = (-\infty, +\infty) \times (-h, h)$ containing a centered initial crack $D = [-l_0, l_0] \times \{0\}$ of length $2l_0$, parallel to its boundaries (Fig. 1a). The non-homogeneous layer Ω_2 represents the heat affected zone (HAZ). The homogeneous layers Ω_1 and Ω_3 represent the weld metal (WM) and the base metal (BM), respectively. Because of the symmetry with respect to the x axis, only the upper half of the structure is modeled. The crack faces are submitted to a uniform anti-plane shear load τ_∞ increasing from 0, and the body forces are neglected. μ_1 and μ_3 are, respectively, the shear modulus of the homogeneous layers Ω_1 and Ω_3. The shear modulus of the non-homogeneous layer $\mu_2(y)$ varies exponentially with the y direction, and the elastic properties are continuous through the interfaces. This variation is given by

$$\mu_2(y) = A\mathrm{e}^{\beta y} \tag{3.1}$$

where

$$\beta = \frac{1}{h_2} \ln \frac{1}{R} \qquad A = \mu_1 \Big(\frac{1}{R}\Big)^{-\frac{h_1}{h_2}} \qquad R = \frac{\mu_1}{\mu_3}$$

and β is the non-homogeneity parameter, the ratio $R = \mu_1/\mu_3$ is referred to as the mismatch ratio.

3.1. Crack growth

The crack is assumed to propagate along the x axis (at $y = 0$) in a symmetrical manner starting from the points $(\pm l_0, 0)$. Thus, we denote by Γ the created crack, and the positions $x = \pm l_a$ correspond to its limits

$$\Gamma = (-l_a, -l_0] \times \{0\} \cup [+l_0, +l_a) \times \{0\} \tag{3.2}$$

The crack evolution follows the Dugdale-Barenblatt model. In other words, the crack faces $(-l_a, -l_0)$ and $(+l_0, +l_a)$ (of the axis $x_2 = 0$) can be divided into two parts:

- The first, close to the crack tip and named the cohesive zone, is subjected to the constant shearing cohesive forces of intensity τ_c.
- The second, named non-cohesive zone, close to the initial crack, without cohesive forces.

These two zones are separated by the limit points $x_1 = \pm l_c$. Note that the values of l_a and l_c depend on the value of the remote loading τ_∞, with hypothesis $l_a \geqslant l_c \geqslant l_0$. At the beginning of loading, we have the initial conditions: $l_a = l_c = l_0$.

In the present case, the crack growth follows two phases: the cohesive crack phase and the propagation phase (Fig. 2). Different criteria of the initiation and propagation of these zones were deduced by Ferdjani *et al.* (2009) from an energy minimization principle. They are presented in the following Sections without demonstration.

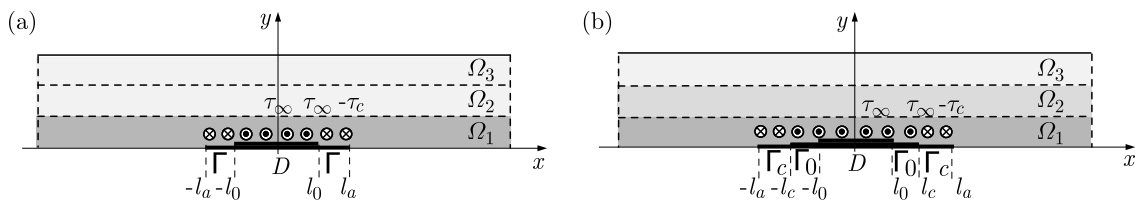

Fig. 2. Evolution of the crack during loading: (a) cohesive phase, (b) propagation phase

3.1.1. Cohesive crack phase

When $\tau_\infty > 0$, a new crack must appear such that the maximum shear stress in the structure remains below the critical value τ_c. As a result, Mode III stress intensity factor K_{III} must be equal to zero at the tip of the crack. At very low values of the loading, the size of the crack is sufficiently small so that the sliding $[|w|]$ becomes everywhere smaller than the critical value δ_c of the Dugdale-Barenblatt model. Consequently, the faces of the newly created crack Γ are submitted to the cohesive forces of intensity τ_c.

The tips $x = \pm l_a$ advance such that the stress level is never above the critical value τ_c in the structure. This implies that the stress is not singular at the front of the crack. As a result, the law governing the evolution of the crack tips at $\pm l_a$ with the loading corresponds to

$$K_{III}(\pm l_a) = 0 \tag{3.3}$$

This phase finishes when the sliding at $x = \pm l_0$ attains the critical value of δ_c. At that moment, a non-cohesive crack appears. The corresponding load will be called the fracture load, and is defined as

$$\tau_r = \sup\{\tau_\infty > 0 : \quad |[|w|](l_0)| < \delta_c\} \tag{3.4}$$

3.1.2. Propagation phase

After the cohesive phase, the equilibrium of the structure cannot be restored without the onset and growth of a non-cohesive part on the faces of the newly created crack. Therefore, the new crack Γ should be divided into two parts, the cohesive part Γ_c and the non-cohesive part Γ_0, their tips are denoted by l_c and l_0, respectively (Fig. 2b)

$$\begin{aligned} &\Gamma = \Gamma_0 \cup \Gamma_c \\ &\Gamma_0 = (-l_c, -l_0] \times \{0\} \cup [l_0, l_c) \times \{0\} \\ &\Gamma_c = (-l_a, -l_c] \times \{0\} \cup [l_c, l_a) \times \{0\} \end{aligned} \tag{3.5}$$

The laws governing the evolution of the tips $\pm l_c$ and $\pm l_a$ are given by

$$K_{III}(\pm l_a) = 0 \qquad |[|w|](\pm l_c)| = \delta_c \tag{3.6}$$

4. Integral equation formulation

The transformation scheme used by Erdogan *et al.* (1973) is used in order to reduce the elastic problem to an integral equation. First, the boundary and transmission conditions of the problem at $y = 0$, $y = h$ and the interfaces ($y = h_1$ and $y = h_1 + h_2$) are presented below

$$\begin{aligned} &y = 0: \quad \tau^1_{yz}(x,0) = \tau(x) \qquad |x| \leqslant l_a \qquad \text{and} \qquad w_1(x,0) = 0 \qquad |x| > l_a \\ &y = h_1: \quad w_1(x,h_1) = w_2(x,h_1) \qquad \tau^1_{yz}(x,h_1) = \tau^2_{yz}(x,h_1) \qquad |x| < +\infty \\ &y = h: \quad \tau^3_{yz}(x,h) = 0 \qquad |x| < +\infty \\ &y = h^* = h_1 + h_2: \quad w_2(x,h^*) = w_3(x,h^*) \qquad \tau^2_{yz}(x,h^*) = \tau^3_{yz}(x,h^*) \qquad |x| < +\infty \end{aligned} \tag{4.1}$$

where $w_i(x,y)$ and τ^i_{yz} are the z-component of the displacement and the stress component in Ω_i, respectively. The loading $\tau(x)$ is given by

$$\tau(x) = \begin{cases} \tau_\infty & \text{for} \quad |x| \leqslant \alpha \\ \tau_\infty - \tau_c & \text{for} \quad \alpha \leqslant |x| \leqslant l_a \end{cases} \tag{4.2}$$

where $\alpha = l_0$ in the cohesive phase and $\alpha = l_c$ in the propagation phase.

Because of the problem symmetry $w_i(x,y) = w_i(-x,y)$ $i = 1,2,3$, we apply the cosine Fourier transforms, and the following expressions are obtained

$$\begin{aligned} w_i(x,y) &= 2\int_0^{+\infty} [C_1^i(\lambda)\mathrm{e}^{n_1 y} + C_2^i(\lambda)\mathrm{e}^{n_2 y}]\cos(\lambda x)\, d\lambda \qquad i = 1,3 \\ w_2(x,y) &= 2\int_0^{+\infty} [C_1^2(\lambda)\mathrm{e}^{r_1 y} + C_2^2(\lambda)\mathrm{e}^{r_2 y}]\cos(\lambda x)\, dx \end{aligned} \tag{4.3}$$

where C_k^j ($k = 1,2$ and $j = 1,3$) are unknown functions of λ to be determined from boundary conditions (4.1). Coefficients n_m and r_m ($m = 1,2$) are the roots of the characteristic polynomial associated with the Laplacian operator. They are given by

$$\begin{aligned} &n_1 = \lambda \qquad\qquad n_2 = -\lambda \\ &r_1 = -\frac{1}{2}\beta - \frac{1}{2}\sqrt{\beta^2 + 4\lambda^2} \qquad r_2 = -\frac{1}{2}\beta + \frac{1}{2}\sqrt{\beta^2 + 4\lambda^2} \end{aligned} \tag{4.4}$$

In order to derive the integral equation, the following density function ψ must be introduced

$$\psi(x) = \frac{\partial}{\partial x}[w_1(x,0^+) - w_1(x,0^-)] = \frac{\partial}{\partial x}[2w_1(x,0^+)] \tag{4.5}$$

It is obvious that the second condition in $(4.1)_1$ would be satisfied if we require

$$\int_{-l_a}^{+l_a} \psi(t)\, dt = 0 \qquad \psi(x) = 0 \qquad \text{for} \qquad |x| \geqslant l_a \tag{4.6}$$

When substituting $(4.3)_1$ into (4.5), accounting for (4.6) and inverting the Fourier integral, we obtain

$$C_1^1(\lambda) + C_2^1(\lambda) = -\frac{1}{2\pi\lambda}\int_0^{+l_a} \psi(t)\sin(\lambda t)\, dt = F \tag{4.7}$$

The first equations in $(4.1)_2$ and in $(4.1)_4$ result in, respectively

$$\begin{aligned} &C_1^1(\lambda)\mathrm{e}^{n_1 h_1} + C_2^1(\lambda)\mathrm{e}^{n_2 h_1} = C_1^2(\lambda)\mathrm{e}^{r_1 h_1} + C_2^2(\lambda)\mathrm{e}^{r_2 h_1} \\ &C_1^3(\lambda)\mathrm{e}^{n_1(h_1+h_2)} + C_2^3(\lambda)\mathrm{e}^{n_2(h_1+h_2)} = C_1^2(\lambda)\mathrm{e}^{r_1(h_1+h_2)} + C_2^2(\lambda)\mathrm{e}^{r_2(h_1+h_2)} \end{aligned} \tag{4.8}$$

The second equations in $(4.1)_2$, $(4.1)_3$ and $(4.1)_4$ give, respectively

$$\begin{aligned} &n_1 C_1^1(\lambda)\mathrm{e}^{n_1 h_1} + n_2 C_2^1(\lambda)\mathrm{e}^{n_2 h_1} = r_1 C_1^2(\lambda)\mathrm{e}^{r_1 h_1} + r_2 C_2^2(\lambda)\mathrm{e}^{r_2 h_1} \\ &n_1 C_1^3(\lambda)\mathrm{e}^{n_1 h} + n_2 C_2^3(\lambda)\mathrm{e}^{n_2 h} = 0 \\ &r_1 C_1^2(\lambda)\mathrm{e}^{r_1(h_1+h_2)} + r_2 C_2^2(\lambda)\mathrm{e}^{r_2(h_1+h_2)} = n_1 C_1^3(\lambda)\mathrm{e}^{n_1(h_1+h_2)} + n_2 C_2^3(\lambda)\mathrm{e}^{n_2(h_1+h_2)} \end{aligned} \tag{4.9}$$

Solving the system of algebraic equations (4.7)-(4.9), gives the two unknown functions $C_1^1(\lambda)$ and $C_2^1(\lambda)$

$$\begin{aligned} C_1^1(\lambda) &= \frac{F\mathrm{e}^{-\lambda h_1}[\mathrm{e}^{\widetilde{h}_2 - \lambda h_3}\mathcal{A}_2 + \mathrm{e}^{-\widetilde{h}_2 - \lambda h_3}\mathcal{A}_1 + \beta(\mathrm{e}^{-\widetilde{h}_2 + \lambda h_3} - \mathrm{e}^{\widetilde{h}_2 + \lambda h_3})]}{Den} \\ C_2^1(\lambda) &= \frac{F\mathrm{e}^{\lambda h_1}[\mathrm{e}^{\widetilde{h}_2 + \lambda h_3}\mathcal{A}_1 + \mathrm{e}^{-\widetilde{h}_2 + \lambda h_3}\mathcal{A}_2 + \beta(\mathrm{e}^{-\widetilde{h}_2 - \lambda h_3} - \mathrm{e}^{\widetilde{h}_2 - \lambda h_3})]}{Den} \end{aligned} \tag{4.10}$$

where

$$\widetilde{h}_2 = \frac{1}{2}\sqrt{\beta^2+4\lambda^2}h_2 \qquad \mathcal{A}_1 = 2\lambda + \sqrt{\beta^2+4\lambda^2} \qquad \mathcal{A}_2 = -2\lambda + \sqrt{\beta^2+4\lambda^2} \tag{4.11}$$

and the denominator Den is given by

$$\begin{aligned} Den = {} & \mathcal{A}_1(\mathrm{e}^{\widetilde{h}_2+\lambda h_3+\lambda h_1} + \mathrm{e}^{-\widetilde{h}_2-\lambda h_3-\lambda h_1}) + \mathcal{A}_2(\mathrm{e}^{\widetilde{h}_2-\lambda h_3-\lambda h_1} + \mathrm{e}^{-\widetilde{h}_2+\lambda h_3+\lambda h_1}) \\ & + \beta(-e^{\widetilde{h}_2-\lambda h_3+\lambda h_1} - \mathrm{e}^{\widetilde{h}_2+\lambda h_3-\lambda h_1} + \mathrm{e}^{-\widetilde{h}_2-\lambda h_3+\lambda h_1} + \mathrm{e}^{-\widetilde{h}_2+\lambda h_3-\lambda h_1}) \end{aligned} \tag{4.12}$$

Using the first boundary condition in $(4.1)_1$, we obtain

$$\int_0^{+l_a} K(x,t)\psi(t)\,dt = -\pi\frac{\tau(x)}{\mu_1} \qquad \text{for} \quad |x| \leqslant l_a \tag{4.13}$$

where

$$K(x,t) = \lim_{y\to 0^+} \int_0^{+\infty} N(y,\lambda)\sin(\lambda t)\cos(\lambda x)\,d\lambda \tag{4.14}$$

and $N(y,\lambda)$ is given by

$$\begin{aligned} N(y,\lambda) = {} & \Big\{\mathrm{e}^{\lambda(y-h_1)}[\mathrm{e}^{\widetilde{h}_2-\lambda h_3}\mathcal{A}_2 + \mathrm{e}^{-\widetilde{h}_2-\lambda h_3}\mathcal{A}_1 + \beta(\mathrm{e}^{-\widetilde{h}_2+\lambda h_3} - \mathrm{e}^{\widetilde{h}_2+\lambda h_3})] \\ & - \mathrm{e}^{\lambda(-y+h_1)}[\mathrm{e}^{\widetilde{h}_2+\lambda h_3}\mathcal{A}_1 + \mathrm{e}^{-\widetilde{h}_2+\lambda h_3}\mathcal{A}_2 + \beta(\mathrm{e}^{-\widetilde{h}_2-\lambda h_3} - \mathrm{e}^{\widetilde{h}_2-\lambda h_3})]\Big\}\frac{1}{Den} \end{aligned} \tag{4.15}$$

Performing an asymptotic analysis for $N(y,\lambda)$ when $\lambda \to \infty$ gives: $N^\infty(y,\lambda) \cong -\mathrm{e}^{-\lambda y}K(x,t)$, and Eq. (4.14) is rewritten as

$$\begin{aligned} K(x,t) = {} & \lim_{y\to 0^+} \int_0^{+\infty} N^\infty(y,\lambda)\sin(\lambda t)\cos(\lambda x)\,d\lambda \\ & + \lim_{y\to 0^+} \int_0^{+\infty} [N(y,\lambda) - N^\infty(y,\lambda)]\sin(\lambda t)\cos(\lambda x)\,d\lambda \\ = {} & \lim_{y\to 0^+} -\int_0^{+\infty} \mathrm{e}^{-\lambda y}\sin(\lambda t)\cos(\lambda x)\,d\lambda + \int_0^{+\infty} [N(0,\lambda)+1]\sin(\lambda t)\cos(\lambda x)\,d\lambda \end{aligned} \tag{4.16}$$

Because of the uniform convergence, the limit in the second integral, Eq. (4.16), has been put under the integral. Thus, by using the relations

$$\begin{aligned} & \lim_{y\to 0^+} \int_0^{+\infty} \mathrm{e}^{-\lambda y}\sin(\lambda t)\cos(\lambda x)\,d\lambda = \frac{t}{(t-x)(t+x)} \\ & k(x,t) = -\int_0^{+\infty} [N(0,\lambda)+1]\sin(\lambda t)\cos(\lambda x)\,d\lambda \end{aligned} \tag{4.17}$$

The singular integral equation in which the only unknown is the function ψ is given by

$$\frac{\mu_1}{\pi}\int_0^{l_a}\Big(\frac{t}{(t-x)(t+x)} + k(x,t)\Big)\psi(t)\,dt = \tau(x) \qquad |x| < l_a \tag{4.18}$$

Because of the parity of the integrand in (4.18), it can be expressed under the following form

$$\frac{\mu_1}{2\pi}\int\limits_{-l_a}^{l_a}\Big(\frac{1}{t-x}+k(x,t)\Big)\psi(t)\,dt=\tau(x)\qquad\qquad |x|<l_a \tag{4.19}$$

with the condition: $\int_{-l_a}^{l_a}\psi(t)\,dt=0$.

In Eq. (4.19), the singular integral is defined in the Cauchy principal value sense.

4.1. Case without HAZ ($h_2=0$)

In order to study the influence of width of the HAZ, we need to model the case without the HAZ (see Fig. 3). Following the same procedure as above, the corresponding singular integral equation is obtained

$$\frac{\mu_1}{2\pi}\int\limits_{-l_a}^{l_a}\Big(\frac{1}{t-x}+k'(x,t)\Big)\psi(t)\,dt=\tau(x)\qquad\qquad |x|<l_a \tag{4.20}$$

with the condition $\int_{-l_a}^{l_a}\psi(t)\,dt=0$, where $k'(x,t)$ is given by

$$k'(x,t)=-\int\limits_0^{+\infty}f(\lambda)\sin(\lambda t)\cos(\lambda x)\,d\lambda \tag{4.21}$$

with

$$f(\lambda)=2\frac{(\mu_1-\mu_3)\mathrm{e}^{\lambda(h_3-h_1)}+(\mu_1+\mu_3)\mathrm{e}^{-\lambda(h_3+h_1)}}{(\mu_1-\mu_3)[\mathrm{e}^{-\lambda(h_3-h_1)}+\mathrm{e}^{\lambda(h_3-h_1)}]+(\mu_1+\mu_3)[\mathrm{e}^{\lambda(h_3+h_1)}+\mathrm{e}^{-\lambda(h_3+h_1)}]}$$

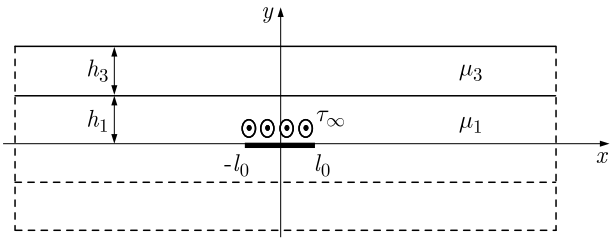

Fig. 3. The studied structure without HAZ

4.2. Integral equation resolution

Let us first introduce the following normalized quantities

$$r=\frac{x}{l_0}\qquad s=\frac{t}{l_0}\qquad \eta=\frac{l_c}{l_a}\qquad \psi(t)=f(s)\qquad k(x,t)=L(r,s) \tag{4.22}$$

Then Eq. (4.19) takes the following form

$$\frac{1}{\pi}\int\limits_{-1}^{1}\Big(\frac{1}{s-r}+l_aL(r,s)\Big)f(s)\,ds=\frac{2}{\mu_1}\tau(r)\qquad\qquad |r|<1 \tag{4.23}$$

with the condition $\int_{-1}^{1}f(s)\,ds=0$.

In Eq. (4.23), the loading $\tau(r)$ is given by

$$\tau(r) = \begin{cases} -\tau_\infty & \text{for} \quad |r| \leqslant \eta \\ -\tau_\infty + \tau_c & \text{for} \quad \eta \leqslant |r| \leqslant 1 \end{cases} \tag{4.24}$$

Loading distribution (4.24) presents jump discontinuities at $\pm\eta$. Thus, following the method proposed by Ioakimidis (1980), $f(s)$ is replaced by a new function $\Phi(s)$ such that

$$f(s) = h(s) + \phi(s) \tag{4.25}$$

where $h(s)$ is the solution to the following integral equation

$$\frac{1}{\pi} \int_{-1}^{+1} \frac{1}{s-r} h(s)\, ds = \frac{2}{\mu_1} \tau(r) \qquad |r| \leqslant 1 \tag{4.26}$$

with the condition $\int_{-1}^{+1} h(s)\, ds = 0$.

The new unknown function $\Phi(s)$ should satisfy the following equation

$$\frac{1}{\pi} \int_{-1}^{+1} \Big(\frac{1}{s-r} + l_a L(r,s) \Big) \phi(s)\, ds = g(r) \qquad |r| \leqslant 1 \tag{4.27}$$

with the condition $\int_{-1}^{+1} \phi(s)\, ds = 0$, where

$$g(r) = -\frac{1}{\pi} \int_{-1}^{+1} l_a L(r,s) h(s)\, ds \tag{4.28}$$

It is obvious from equation (4.28) that, since $L(r,s)$ have regular behavior, the same must hold true for $g(r)$ too, and the numerical techniques for the resolution of singular integral equations can be directly applied to solve equations (4.27) and (4.28) without any modifications (Ioakimidis, 1980). The solution $f(s)$ of Eq. (4.23) will be given by Eq. (4.25). The closed-form solution to equation (4.26) was determined by Gakhov (1966) as follows

$$h(s) = -\frac{2}{\pi\mu_1} \frac{1}{\sqrt{1-s^2}} \int_{-1}^{+1} \sqrt{1-r^2}\, \frac{\tau(r)}{r-s}\, dr \tag{4.29}$$

By performing integration in (4.29) in the closed form, we obtain

$$h(s) = h_1(s) + h_2(s) \tag{4.30}$$

where

$$\begin{aligned} h_1(s) &= \frac{2s}{\pi\mu_1} \frac{1}{\sqrt{1-s^2}} (-\pi\tau_\infty + 2\tau_c \arccos\eta) \\ h_2(s) &= \frac{2\tau_c}{\pi\mu_1} \ln \left| \frac{\eta\sqrt{1-s^2} - s\sqrt{1-\eta^2}}{\eta\sqrt{1-s^2} + s\sqrt{1-\eta^2}} \right| \end{aligned} \tag{4.31}$$

Singular integral equation (4.27) has an index 1 because the unknown function $\Phi(s)$ presents integrable singularities at the end points ± 1 (Erdogan *et al.*, 1973). The solution can be expressed as $\Phi(s) = w(s)\psi(s)$, where $w(s) = 1/\sqrt{1-s^2}$ is the weight function associated with the Tchebychev polynomials of the first kind $T_n(s) = \cos(n \arccos s)$. $\psi(s)$ is a continuous and bounded

function in the interval $[-1,1]$ which may be expressed as a truncated series of Tchebychev polynomials of the first kind. It is clear from the problem symmetry that $\Phi(-s) = -\Phi(s)$. Then, the solution to (4.27) may be expressed as

$$\phi(s) = \frac{1}{\sqrt{1-s^2}} \sum_{i=1}^{N} A_i T_{2i-1}(s) \tag{4.32}$$

When substituting (4.32) into (4.27) and making use of the following relation

$$\frac{1}{\pi} \int_{-1}^{+1} \frac{T_i(s)}{\sqrt{1-s^2}(s-r)}\, ds = \begin{cases} U_{i-1}(r) & i > 0 \\ 0 & i = 0 \end{cases} \tag{4.33}$$

where $U_i(r) = \sin[(i+1)\arccos(r)]\sqrt{1-s^2}$ designates the Tchebychev polynomials of the second kind. We find

$$\sum_{i=1}^{N} A_i [U_{2i-2}(r) + H_i(r)] = g(r) \tag{4.34}$$

where

$$H_i(r) = \frac{1}{\pi} \int_{-1}^{1} \frac{1}{\sqrt{1-s^2}} l_a L(r,s) T_{2i-1}(s)\, ds \tag{4.35}$$

Equation (4.34) may be solved by selecting a set of N collocation points, given by

$$r_j = \cos\frac{(2j-1)\pi}{2(2N-1)} \qquad \text{for} \quad j = 1, \ldots, N \tag{4.36}$$

Using the collocation points given by equation (4.36) in equation (4.34) yields a system of N equations with N unknowns, namely $A_1, \ldots, A_N$ which may be expressed as

$$\sum_{i=1}^{N} A_i [U_{2i-2}(r_j) + H_i(r_j)] = g(r_j) \qquad j = 1, \ldots, N \tag{4.37}$$

Mode III stress intensity factor is given by the following formula (Cherepanov, 1979)

$$K_{III}(\pm l_a) = \sqrt{l_a}\frac{\mu_1}{2} \lim_{x \to \pm l_a} \sqrt{l_a^2 - x^2}\psi(x) = \sqrt{l_a}\frac{\mu_1}{2} \lim_{s \to \pm 1} \sqrt{1-s^2} f(s) \tag{4.38}$$

The following result is obtained

$$K_{III}(\pm l_a) = \sqrt{l_a}\Big(\tau_\infty - \frac{2}{\pi}\tau_c \arccos\frac{l_c}{la} - \frac{\mu_1}{2}\sum_{i=1}^{N} A_i\Big) \tag{4.39}$$

The relative crack sliding at a point x in the interval $[-l_a, l_a]$ is defined by

$$\delta(x) = w(x, 0^+) - w(x, 0^-) = \int_{-l_a}^{x} \psi(t)\, dt \tag{4.40}$$

We obtain from (4.22), (4.25), (4.30) and (4.31)

$$\delta(x) = \frac{2}{\pi\mu_1}\left[\pi\tau_\infty\sqrt{l_a^2-x^2} + \tau_c\left(x\ln\left|\frac{x\sqrt{l_a^2-l_c^2} - l_c\sqrt{l_a^2-x^2}}{x\sqrt{l_a^2-l_c^2} + l_c\sqrt{l_a^2-x^2}}\right|\right.\right.$$
$$\left.\left. + l_c\ln\left|\frac{(\sqrt{l_a^2-x^2}+\sqrt{l_a^2-l_c^2})^2}{x^2-l_c^2}\right|\right) - 2\sqrt{l_a^2-x^2}\arccos\frac{l_c}{l_a}\right] \tag{4.41}$$
$$- \sqrt{l_a^2-x^2}\sum_{i=1}^{N}\frac{A_i U_{2i-2}(x/l_a)}{2i-1}$$

To obtain (4.41), the following relation was used

$$\int_{-1}^{s}\frac{T_i(x)}{\sqrt{1-x^2}}\,dx = -\frac{1}{i}U_{i-1}(s)\sqrt{1-s^2} \tag{4.42}$$

From equation (4.41), the crack sliding at $x = \pm l_c$ is given by

$$\delta(\pm l_c) = \frac{2l_a}{\pi\mu_1}\Big[\pi\sqrt{1-\eta^2}\Big(\tau_\infty - \frac{2\tau_c}{\pi}\arccos\frac{l_c}{l_a}\Big) - 2\tau_c\eta\ln\eta\Big] - l_a\sqrt{1-\eta^2}\sum_{i=1}^{N}\frac{A_i U_{2i-2}(\pm\eta)}{2i-1} \tag{4.43}$$

5. Results and discussion

The problem can be described with a set of the following dimensionless parameters: μ_1/τ_c, μ_3/τ_c, h_1/l_0, h_2/l_0, h_3/l_0 and δ_c/l_0. In this Section, we present parametric studies carried out by varying these parameters.

5.1. Influence of the mismatch ratio μ_1/μ_3

In this Section, the dimensionless parameters are set to the following values

$$\frac{h_1}{l_0} = 3 \qquad \frac{h_2}{l_0} = 4 \qquad \frac{h_3}{l_0} = 7 \qquad \frac{\delta_c}{l_0} = 0.001$$

For the other parameters, two cases are considered:

- Case 1: $\mu_1/\tau_c = 100$ and μ_3/τ_c variable.
- Case 2: $\mu_3/\tau_c = 100$ and μ_1/τ_c variable.

The evolution of τ_∞ with the crack length l_c is given in Fig. 4 for the two cases and for three values of μ_1/μ_3: 0.1, 1 and 10. For all the curves, the vertical part corresponds to the cohesive phase when $l_c = l_0$, and the decreasing part corresponds to the propagation phase. The maximum load for each curve is the fracture load τ_r. We notice from Fig. 4a that in the first case, the crack propagation has a relatively negligible sensitivity to the mismatch ratio. While, for the second case (see Fig. 4b), we notice a strong sensitivity to the mismatch ratio. This means that, for the crack propagation, the rigidity of the weld joint is much more important than that of the base metal. To emphasize this phenomenon, the variation of the fracture load with the mismatch ratio for the two cases is presented in Fig. 5. It is observed that the fracture load is very sensitive to the rigidity of the weld joint, whereas it is practically insensitive to the one of the base metal.

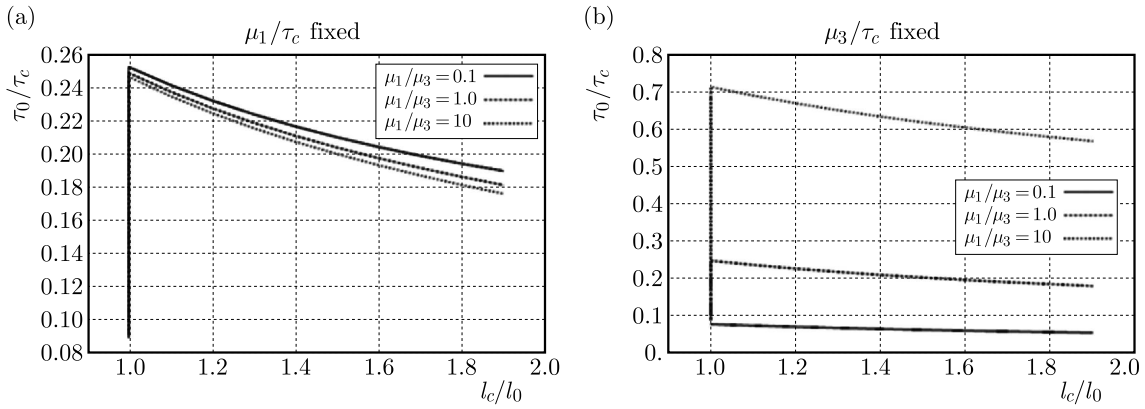

Fig. 4. Evolution of τ_∞ with the crack length l_c for the two cases and for three values of the mismatch ratio

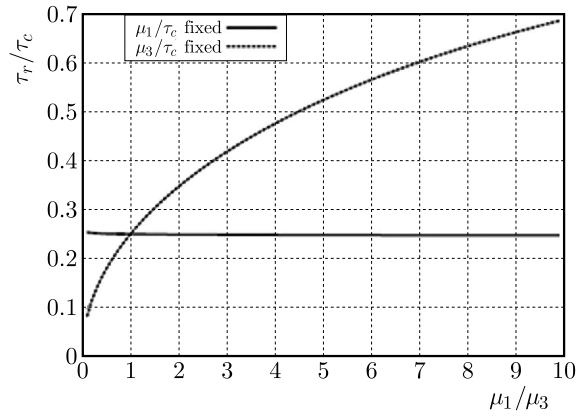

Fig. 5. Evolution of τ_r/τ_c with the mismatch ratio μ_3/μ_1

5.2. Influence of the HAZ width

In the precedent paragraphs, width of the HAZ has been arbitrarily set to the value $h_2/l_0 = 4$. In order to quantify the influence of this width on the results, the fracture load was computed for different values of h_2/l_0 (h/l_0 and h_1/l_0 fixed) (see Fig. 1a). The dimensionless parameters were set to the following values

$$\frac{h_1}{l_0} = 3 \qquad \frac{h}{l_0} = 14 \qquad \frac{\delta_c}{l_0} = 0.001 \qquad \frac{\mu_1}{\mu_3} = \frac{1}{2}$$

It is seen in Fig. 6 that for a given weld metal width, the fracture load is a decreasing function of width of the HAZ. It is also noticed that the influence of this parameter is negligible.

Indeed, for the case $h_2 = 0$ (without HAZ), the value of the relative fracture load τ_r/τ_c is 0.251. While it is 0.249 for $h_2/(h_2 + h_3) = 1$ (without BM), making a relative difference of 0.8%.

In order to see if this influence is also negligible for the crack propagation, the evolution of the applied load with the crack length is represented in Fig. 7 for two extreme values of width of the HAZ. It is seen that the two curves are close to each other, which confirms the weak influence of this parameter observed for the fracture load.

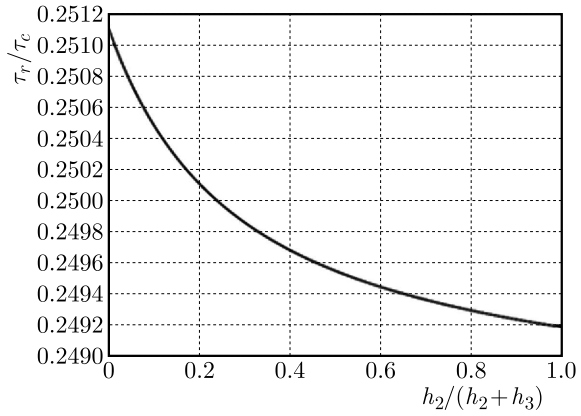

Fig. 6. Evolution of τ_r/τ_c with the HAZ width h_2

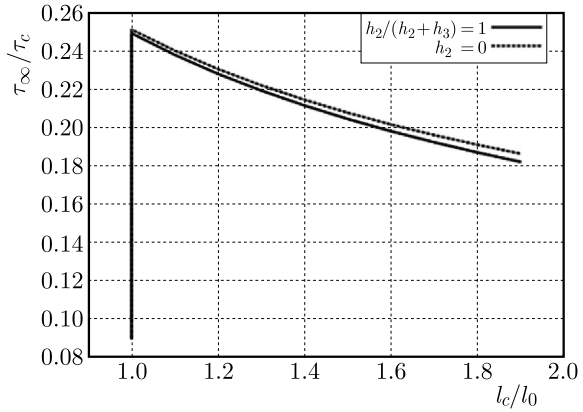

Fig. 7. Evolution of the applied load τ_∞ with the crack length l_c for two extreme values of the HAZ width

6. Conclusions

The most important results of this work are the following:

- The problem of a Dugdale-Barenblatt crack in a welded strip under anti-plane shear loading was reduced to a singular integral equation solved semi-analytically.
- The crack propagation was modeled and the fracture load was calculated for different values of the problem parameters.
- It was found that the influence of the mismatch ratio μ_1/μ_3 was very important when the parameter μ_3/τ_c (relative rigidity of the base metal) was fixed. While it was negligible when μ_1/τ_c (relative rigidity of the weld metal) was fixed.
- The influence of the heat affected zone width is negligible. Consequently, the HAZ can be completely omitted from the modelization without significant consequences.

References

1. Burstow M.C., Howard I.C., Ainsworth R.A., 1998, The effects of material strength mismatching on constraint at the limit load of welded three-point bend specimens, *International Journal of Fracture*, **89**, 2, 117-142

2. Cherepanov G.P., 1979, *Mechanics of Brittle Fracture*, New York: McGraw-Hill International Book Co.

3. Donato G.H.B., Magnabosco R., Ruggieri C., 2009, Effects of weld strength mismatch on J and CTOD estimation procedure for SE(B) specimens, *International Journal of Fracture*, **159**, 1-20
4. Erdogan F., Gupta G.D., Cook T., 1973, Numerical solution of singular integral equation, [In:] *Methods of Analysis and Solutions of Crack Problems*, G.C. Sih (Edit.), Noordhoff International Publishing, Leyden, 368-425
5. Ferdjani H., 2008, Study of an infinite strip containing a Dugdale crack parallel to its boundaries under antiplane shear loading, *European Journal of Mechanics, A/Solids*, DOI: 10.1016/j.euromechsol.2008.07.001
6. Ferdjani H., 2013, Dugdale Crack at the interface of two different materials under antiplane shear loading, *Key Engineering Materials*, **550**, 63-70
7. Ferdjani H., Abdelmoula R., Marigo J.-J., 2007, Insensitivity to small defects of the fracture of materials governed by the Dugdale model, *Continuum Mechanics and Thermodynamics*, **19**, 191-210
8. Ferdjani H., Abdelmoula R., Marigo J.-J., El Borgi S., 2009, Study of size effects in the Dugdale model through the case of a crack in a semi-infinite plane under anti-plane shear loading, *Continuum Mechanics and Thermodynamics*, **21**, 41-55
9. Ferdjani H., Marigo J.-J., 2015, Application of the Dugdale's model to a mixed mode loading of a semi infinite cracked structure, *European Journal of Mechanics, A/Solids*, **53**, 1-9
10. Francfort G.A., Marigo J.J., 1998, Revisiting brittle fracture as an energy minimization problem, *Journal of the Mechanics and Physics of Solids*, **46**, 8, 1319-1342
11. Gakhov F.D., 1966, *Boundary Value Problems*, Pergamon Press and Addison-Wesley, Oxford
12. Hao S., Cornec A., Schwalbe K.-H., 1997, Plastic stress-strain fields and limit loads of a plane strain cracked tensile panel with a mismatched welded joint, *International Journal of Solids and Structures*, **34**, 3, 297-326
13. Hao S., Schwalbe K.-H., Cornec A., 2000, The effect of yield strength mis-match on the fracture analysis of welded joints: slip-line field solutions for pure bending, *International Journal of Solids and Structures*, **37**, 5385-5411
14. Ioakimidis N.I., 1980, The numerical solution of crack problems in plane elasticity in the case of loading discontinuities, *Engineering Fracture Mechanics*, **13**, 709-716
15. Li Y.-D., Zhang H.-C., Tan W., Lee K.Y., 2008, Mechanical modeling and fracture analysis for a non-homogeneous weldment with a crack perpendicular to the interface, *International Journal of Solids and Structures*, **45**, 5730-5743
16. Negre P., Steglich D., Brocks W., 2004, Crack extension in aluminum welds: a numerical approach using the Gurson-Tvergaard-Needleman model, *Engineering Fracture Mechanics*, **71**, 2365-2383
17. Rakin M., Gubeljak N., Dobrojevic M, Sedmak A., 2008, Modelling of ductile fracture initiation in strength mismatched welded joint, *Engineering Fracture Mechanics*, **75**, 3499-3510
18. Ranestad Ø., Thaulow C., Zhang Z.L., 1997, Two-parameter (J-M) description of crack tip stress-fields for an idealized weldment in small scale yielding, *International Journal of Fracture*, **88**, 315-333
19. Zhang M., Shi Y.-W., Zhang X.P., 1997a, Influence of strength mis-matching on crack driving force and failure assessment curve of weldment, *International Journal of Pressure Vessels and Piping*, **70**, 33-41
20. Zhang Z.L., Thaulow C., Hauge M., 1997, Effects of crack size and weld metal mismatch on the HAZ cleavage toughness of wide plates, *Engineering Fracture Mechanics*, **57**, 6, 653-664

Manuscript received April 8, 2018; accepted for print January 28, 2019